ACS APPLIED MATERIALS & INTERFACES

Research Article

www.acsami.org

Thin-Film Copper Indium Gallium Selenide Solar Cell Based on Low-Temperature All-Printing Process

Manjeet Singh,* Jinting Jiu,* Tohru Sugahara, and Katsuaki Suganuma

Department of Advanced Interconnection Materials, Institute of Scientific and Industrial Research, Osaka University Mihogaoka 8-1, Ibaraki, Osaka 567-0047, Japan

Supporting Information

ABSTRACT: In the solar cell field, development of simple, low-cost, and low-temperature fabrication processes has become an important trend for energy-saving and environmental issues. Copper indium gallium selenide (CIGS) solar cells have attracted much attention due to the high absorption coefficient, tunable band gap energy, and high efficiency. However, vacuum and high-temperature processing in fabrication of solar cells have limited the applications. There is a strong need to develop simple and scalable methods. In this work, a CIGS solar cell based on all printing steps and low-temperature annealing is developed. CIGS absorber thin film is deposited by using dodecylamine-stabilized CIGS nanoparticle ink followed by printing buffer layer. Silver nanowire (AgNW) ink and sol−gel-derived ZnO precursor solution are used to prepare a highly conductive window layer ZnO/[AgNW/ZnO] electrode with a printing method that achieves 16 Ω/sq sheet resistance and 94% transparency. A CIGS solar cell based on all printing processes exhibits efficiency of 1.6% with open circuit voltage of 0.48 V, short circuit current density of 9.7 mA/cm^2, and fill factor of 0.34 for 200 nm thick CIGS film, fabricated under ambient conditions and annealed at 250 °C.

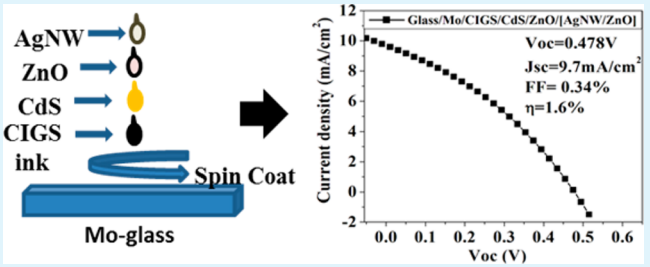

KEYWORDS: *CIGS nanoparticles, low temperature, printing process, Ag nanowires, ZnO sol−gel*

1. INTRODUCTION

With global population growth and increased energy consumption, how to effectively use clean solar energy without depletion has become one of the urgent world research issues. Solar cells, such as silicon, GaN, dye-sensitized, and copper indium gallium selenide (CIGS), have been extensively studied and applied recently. Among these cells, a thin-film CIGS solar cell has attracted much attention due to its high efficiency, band gap tunability, and cell stability.[1] The most efficient CIGS solar cell is based on harsh fabrication processing, such as high-vacuum deposition, high selenization temperature, and complicated multilayer structure.[2] These complicated and high-cost fabrication processes have greatly stimulated the development of solution techniques, such as printing and electrodeposition. A vacuum-free, simple, low-cost and low-temperature printing process has become an important goal for fabrication of CIGS solar cells. Normally, a CIGS solar cell includes three parts: a CIGS absorber layer, a buffer layer, and a conductive window layer. Owing to large-scale production and low-cost processing, the simplest low-temperature solar cell can be fabricated when all these layers become printable. For example, concerning the CIGS absorber layer, recently several solution ink methods have been developed[3−8] and efficiency of 15.2% has been achieved. However, highly toxic materials like hydrazine and high-temperature postdeposition annealing have been employed.[8] In order to prevent the use of toxic compounds, other simple solution-phase methods have been developed for synthesis of CIGS nanoparticle ink for solution-process deposition by using long-chain oleylamine as solvent and dispersant to prepare CIGS nanoparticles due to its better dispersion ability and high boiling point.[9−14] Panthani et al.[15] first prepared an oleylamine-stabilized CIGS nanocrystal ink-based cell and reported 0.2% efficiency with an intrinsic zinc oxide/indium tin oxide (i-ZnO/ITO) top window layer deposited by a radio frequency (rf) sputtering method without any postdeposition high-temperature treatment of CIGS film. Akhavan et al.[16] demonstrated 3% efficiency for spray-coated $CuInSe_2$ nanocrystals film as absorber materials, but after heat treatment of the completed cell in vacuum at 200 °C for 40 min. The major problem with using long-chain amine to synthesize CIGS nanoparticles has been the formation of an insulating layer on the nanoparticle surface, which limits the sintering nanoparticles at low temperature.[13,14,17] All these CIGS nanoparticle films were annealed in vacuum[16] or some others were annealed under Se atmosphere at high temperature.[18] Additionally, due to recombination of photogenerated carriers at the surface insulating layer, surface passivation of CIGS is required in order to achieve substantial device performance for commercial uses. A solvent with smaller carbon chain and low boiling point may be a better alternative

Received: July 10, 2014
Accepted: September 2, 2014
Published: September 2, 2014

to prepare surface-modified CIGS grains due to easy removal from the surface of CIGS nanoparticles at low temperature. Consequently, it is required to develop a modified method of CIGS synthesis and to extend its use in an all-layers-printed solar cell without any vacuum-based processing and high-temperature treatments.

For CdS buffer layer deposition, chemical bath deposition (CBD) has been the most common route.[19] Nevertheless, the problem with CBD is the loss of materials. Hence, a spin-coating method has been reported to decrease the loss of materials after the deposition process.[20]

In addition to the solution-process deposition of CIGS and CdS layers, formation of a window layer on top of the CIGS layer also determines the cost and efficiency of the cells. Normally, a vacuum-deposited i-ZnO/Al·ZnO or ITO layer has been the main candidate as window layer and to maintain the strong adhesion between window layer and absorber layer, which facilitates charge carrier transfer. However, multilayer deposition processing using different deposition techniques largely complicates the fabrication of cells and increases the cost.

To replace the vacuum-based costly i-ZnO/Al·ZnO or ITO deposition, various other transparent electrode materials have been employed in manufacturing of solar cells.[21−25] Recently, silver nanowire (AgNW) films have been demonstrated as an alternative to vacuum-deposited transparent conductive oxide as top contact electrode[26−29] materials. However, weak adhesion and smaller contact area between AgNWs and n-type buffer layer leads to the incapability of collecting charge carriers generated at the p−n junction. Other oxide compounds such as ZnO, Al·ZnO, and ITO have been used to improve the conductivity of AgNW/oxide composite films and adhesion with n-type materials.[30,31] For example, Kim et al.[30] demonstrated solution-processed high-quality top conductive oxide electrodes structured as Al·ZnO/AgNW/Al·ZnO/ZnO stacked layers. They prepared ZnO and Al·ZnO films by sol−gel combustion at 200 °C, which may deteriorate the performance of AgNWs. Chung et al.[31] demonstrated use of AgNWs with expensive and scarce ITO nanoparticle-stacked composite as top electrode to fabricate vacuum-deposited CIGS solar cell. These electrodes[30,31] suffered from low transparency and high resistance due to the use of multiple coating cycles and nanoparticles. Nevertheless, these results confirmed that AgNW film is a promising candidate for window layer. However, these solution-processed window layers were assembled on top of vacuum-deposited CIGS layers and demonstrated those interface interactions. Until now, there has been no report in literature demonstrating the deliberate arrangement of solution-processed CIGS absorber and solution-processed window layer, that is, an all-layers solution-processed CIGS solar cell.

In order to fabricate a low-cost all-layers-printed CIGS solar cell device, we present CIGS nanoparticle synthesis in short carbon chain dodecylamine (DDA) to prepare absorber layer sintered at low temperature (250 °C) in an atmospheric environment, followed by coating of CdS layer and a solution-processed ZnO/[AgNW/ZnO] composite layer as top transparent window electrode. For the first time, we are demonstrating the use of DDA-stabilized CIGS nanoparticles for solar cell fabrication. In addition, the performance of an all-layers-printed CIGS solar cell structured as glass/Mo/CIGS/CdS/ZnO/[AgNW/ZnO] is demonstrated and evaluated.

2. EXPERIMENTAL SECTION

2.1. Synthesis of CIGS Nanoparticles and Fabrication of CIGS Solar Cell. CuCl [copper(I) chloride, 5 mmol], $InCl_3$ [indium(III) chloride, 3.5 mmol], $Ga(acac)_3$ [gallium acetyl acetonate, 1.5 mmol], and elemental Se (selenium, 10 mmol) were mixed in 20 mL of DDA as a coordinating solvent to prepare CIGS nanoparticles. All the chemicals were purchased from Wako Chemicals Industry, Japan. The flask with attached condenser, containing all the precursors in DDA, was heated up to 80 °C for 10 min on a hot plate with vigorous stirring and continuous nitrogen flow. The temperature of the reaction mixture was increased up to 240 °C with vigorous stirring and continued at this temperature for 4 h. A dark black, thick solution was obtained as product. The product solution was precipitated, washed in methanol and toluene, and centrifuged at 8000 rpm to remove excess DDA. Any desired composition of CIGS nanoparticles can be prepared by use of DDA. Details of synthesis parameters and properties of various compositions of CIGS nanoparticles prepared in DDA can be found in our recent publication.[32] CIGS nanoparticles were suspended in *o*-dichlorobenzene at a concentration of 50 mg/mL to fabricate CIGS film by spin-coating. Thin film with thickness of 200 nm was prepared by spin-coating CIGS ink solution at 1500 rpm for 30 s. Finally, prepared CIGS film was annealed at 250 °C for 30 min to remove DDA and impurities present in the film and to improve contact between CIGS and Mo substrate. After that, the CdS film was deposited by use of precursor solution by spin-coating.[20]

The top conductive oxide window electrode was prepared by using AgNWs and sol−gel-derived ZnO precursor solution. AgNWs were synthesized by the well-known polyol process[33,34] as earlier reported by our group. The AgNWs were 50 nm in diameter and 60 μm in length. To prepare ZnO precursor solution, (1 M) zinc acetate [$Zn(CH_3COO)_2{\cdot}2H_2O$] were dissolved in 2-methoxyethanol ($CH_3OCH_2CH_2OH$) and monoethanolamine ($NH_2CH_2CH_2OH$). Equimolar amounts of zinc acetate and monoethanolamine were used. After being stirred for 2−3 h, the solution was kept for 2 days for aging. The transparent solution obtained after aging is the ZnO precursor solution.

After deposition of CIGS and CdS layers for the all-printed CIGS solar cell, the top conductive electrode ZnO/[AgNW/ZnO] was deposited by solution coating. ZnO precursor solution was spin-coated four times at 2000 rpm for 30 s. After each coating, film was dried at 250 °C for 5 min. Above ZnO layer, AgNW solution (2 wt %) was spin-coated two times at 1000 rpm for 20 s and dried at room temperature. Again one layer of ZnO was coated over AgNW and dried at 200 °C for 5 min. At last, a cell based on the structure of glass/Mo/CIGS/CdS/ZnO/[AgNW/ZnO] was fabricated by all-printed methods. Cells with active area of 0.1 cm^2 were prepared by mechanical scribing for measurement.

2.2. Characterization. The CIGS nanoparticles were characterized by transmission electron microscopy (TEM), scanning electron microscopy (SEM), and X-ray diffraction (XRD). TEM imaging (JEOL-JSM at accelerating voltage of 300 kV) of the CIGS nanoparticles was done by placing a drop of toluene suspension on a Cu grid. SEM and energy-dispersive spectrometry (EDS) (JEOL-JSM at accelerating voltage of 5 kV) analysis were done by drying the powder sample on glass. XRD of the powder and film was performed on a Rigaku Rapid II X-ray diffractometer in 2θ range from 10° to 80° with scan speed of 6 deg/min with Cu target (Cu Kα radiation λ = 1.54 Å). Thermogravimetric analysis (TGA) (Netzsch TG-DTA 200SE) was carried out by collecting powder removed from glass substrate.

Optical transmittance of the ZnO/[AgNW/ZnO] composite electrode was measured at room temperature on a UV−vis spectrophotometer (Jasco V-670) in the wavelength range from 300 to 1400 nm. XRD was carried out to check the crystallinity of the composite electrode. The surface morphology of ZnO/[AgNW/ZnO] composite electrode was analyzed by a scanning electron microscope and atomic force microscopy (Nanoscope SII, Nanocute). The sheet resistances of the ZnO/[AgNW/ZnO] samples were measured by a four-point probe system (LorestaGP T610, Mitsubishi Chemical

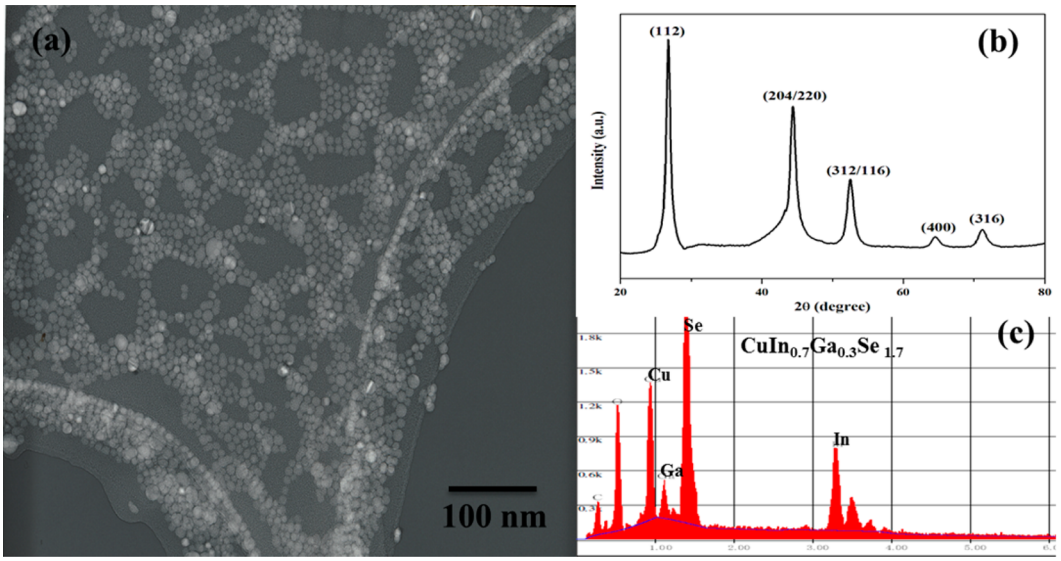

Figure 1. (a) TEM image, (b) XRD pattern, and (c) SEM−EDS spectra of synthesized DDA-stabilized CIGS nanoparticles.

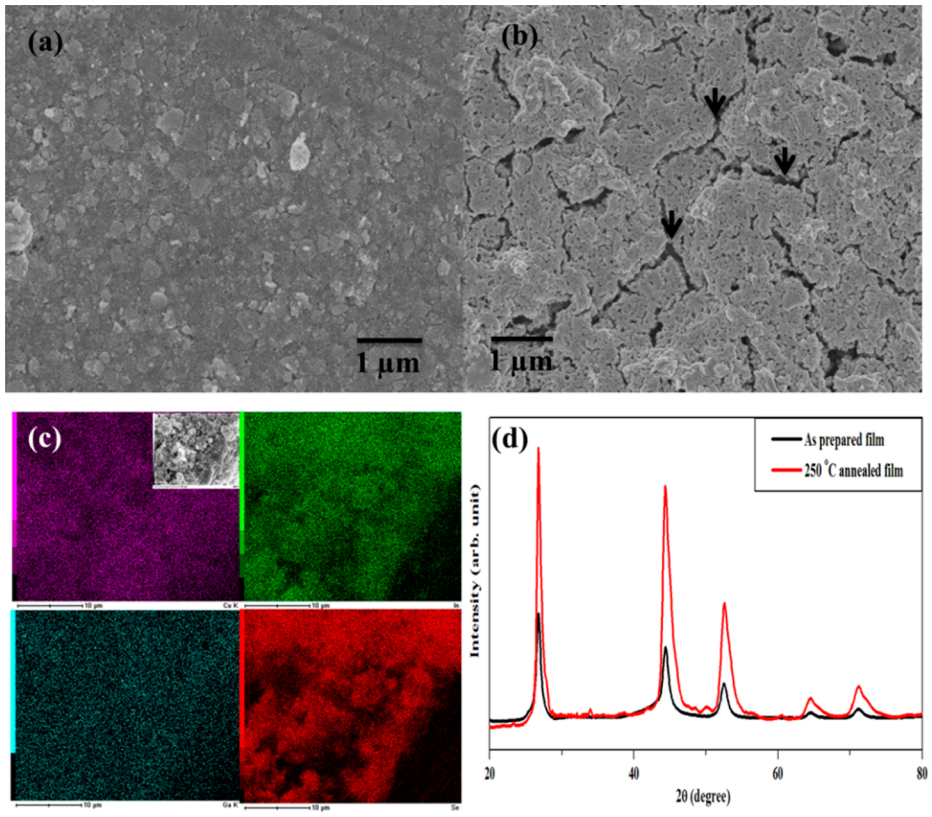

Figure 2. (a, b) SEM images of the surface of (a) as-prepared CIGS film on glass and (b) film heated at 250 °C for 30 min. (c) Elemental mapping image of CIGS film heated at 250 °C. (d) Comparison of XRD patterns of as-prepared CIGS film and film heated at 250 °C.

Analytech Co. Ltd.). The resistance reported here is the average value obtained after at least 10 measurements. The efficiency of the device fabricated with structure glass/Mo/CIGS/CdS/ZnO/[AgNW/ZnO] was measured by Keithley 2400 solar simulator under AM1.5 illumination.

3. RESULTS AND DISCUSSION

Figure 1 presents the TEM image, XRD pattern, and EDS results of as-synthesized DDA-stabilized CIGS nanoparticles. TEM image (Figure 1a) shows the spherical particles in size range from 15 to 20 nm. XRD pattern (Figure 1b) shows the presence of phase-pure CIGS nanoparticles, as peak splitting was not observed. Intensity of the XRD peaks clearly indicates well-crystallized particles. The average crystallite size calculated from Scherrer formula was obtained as 18 nm, which is in good agreement with TEM results. EDS analysis of the CIGS nanoparticles (Figure 1c) reveals the composition as $CuIn_{0.7}Ga_{0.3}Se_{1.7}$. It is interesting to observe that the size of DDA-stabilized CIGS nanoparticles is same as prepared in

longer carbon chain containing solvents such as widely used oleylamine.[15]

CIGS nanoparticle ink was coated on the Mo substrate to achieve a thin film of 200 nm thickness. Figure 2 presents morphology of the thin film prepared from DDA-stabilized CIGS nanoparticle ink. Figure 2 shows the surface morphology of (a) the thin film deposited from as-prepared DDA-stabilized CIGS nanoparticles and (b) the film heated at 250 °C for 30 min. As-prepared CIGS film (Figure 2a) shows aggregated fine particles, and the film remained homogeneous without cracks. After heating at 250 °C for 30 min, cracks were observed (marked by arrow in Figure 2b) in the film, which suggested that the film shrank due to removal of DDA and the surface appeared more compact due to close contact among the particles. The composition of CIGS was obtained as $CuIn_{0.7}Ga_{0.3}Se_{1.7}$ for as-prepared film and $Cu_{0.8}In_{0.7}Ga_{0.2}Se_{1.6}$ for film heated at 250 °C. EDS spectra are shown in Figure S1 in Supporting Information. The change in composition indicated that, during heating at 250 °C, there was elemental loss in the film and the composition changed to Cu-poor after heating. The removal of DDA after the film was heated at 250 °C was confirmed by carbon content in the film, which decreased from 30 to 6 at. % as revealed by the EDS spectra (Figure S1, Supporting Information). TGA curve of the CIGS nanoparticles (Figure S2, Supporting Information) reveals that the weight loss is about 50% below 250 °C. Most of the weight loss is associated with carbon loss because there is no other reaction that can happen under the present conditions. The decrease in oxygen content was also observed after the film was heated at 250 °C for 30 min, as revealed by EDS spectra (Figure S1, Supporting Information). This decrease in oxygen may be due to the conversion of oxide impurities into CIGS phase due to chemical reaction during the sintering process. The cross section image (Figure S3, Supporting Information) of CIGS film after heating at 250 °C shows a dense film with 200 nm thickness. We intentionally prepared a very thin CIGS film so that it could be annealed at low temperature and could form better adhesion with Mo-glass substrate. The cost of the cell could also be minimized by making a very thin film in comparison with conventional 2−3 μm thick film. Figure 2c presents elemental mapping of the as-prepared CIGS film. It indicates the uniform presence of all four elements throughout the film. Figure 2d shows the XRD patterns of as-prepared CIGS film and film annealed at 250 °C for 30 min. It is clear from the figure that the intensity of XRD peaks increases after heating as compared to as-prepared film. Increase in intensity is again attributed to the removal of DDA and increase in crystallite size of CIGS due to sintering of nanoparticles. Thus, it is clear that DDA-stabilized CIGS film can be annealed at low temperature due to easy removal of DDA.

CIGS cell is a multilayer structure including CIGS absorber, CdS buffer layer, and top transparent conductive oxide window electrode. At higher temperature, large amounts of Cd from the CdS layer diffuse into the CIGS layer, and also Se from the CIGS layer reacts with n-type CdS to form CdSe, which no longer remains n-type material. Normally, high-temperature annealing of the CIGS absorber layer in Se atmosphere is used to restrain the diffusion of Se, and then rf sputtering at about 200 °C is used to deposit top conductive oxide electrode in many reports.[30,31] In the present work, low-temperature-processed CIGS layer is deposited, followed by CdS layer deposition and solution-processed top conductive oxide electrode structured as ZnO/[AgNW/ZnO] at 200−250 °C temperature. The thickness of the bottom ZnO layer near the CdS layer was optimized to achieve highest transparency and lowest sheet resistance in composite electrode ZnO/[AgNW/ZnO]. The role of the top ZnO layer in ZnO/[AgNW/ZnO] electrode was to cover AgNWs and to fill in the gap between wires, making the composite film more conductive as described in the Introduction. Figure 3 shows UV−vis transmittance

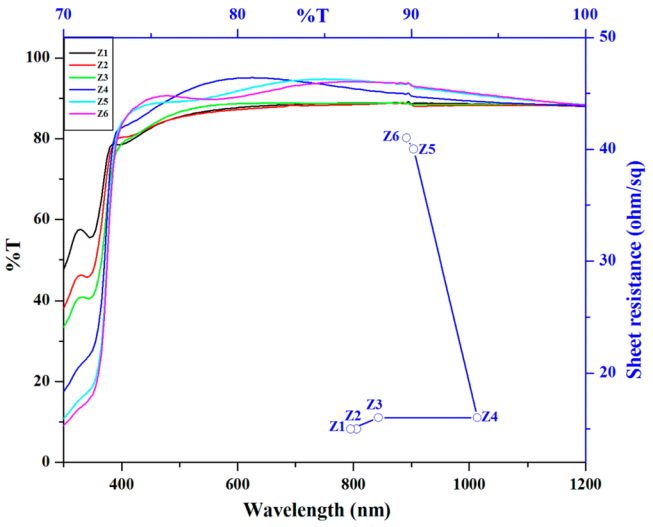

Figure 3. UV−vis transmittance curve of ZnO/[AgNW/ZnO] composite electrode at different coating cycles (represented as Z1−Z6 for 1−6 cycles of spin-coating, respectively) and the plot of sheet resistance (Ω/sq) vs % *T* for samples Z1−Z6 (left *y*-axis and top *x*-axis, shown in blue).

curves of ZnO/[AgNW/ZnO] at different coating cycles (represented as Z1−Z6 for 1−6 cycles of spin-coating, respectively) for the bottom ZnO layer while the upper [AgNW/ZnO] layer was kept the same. Figure 3 also presents the change of sheet resistance with transmittance (blue line), plotted on left *y*-axis and top *x*-axis. Figure 3 reveals that up to three coating cycles the transparency is about the same (88% at 550 nm), but for the fourth ZnO coated layer (sample Z4), transparency increases dramatically to 94% at 550 nm and is higher than 92% in the range from 500 to 700 nm. The thickness of the ZnO layer was about 200 nm after four cycles of spin-coating with precursor solution (Figure S4, Supporting Information). This thickness of ZnO is enough to improve the roughness of lower-lying CdS−CIGS surface for a high-performance solar cell. As the number of coatings increased, transparency was found to decrease for five and six coating cycles and drop to 90% at 550 nm. The values of sheet resistance for the samples were measured as 15, 15, 16, 16, 40, and 41 Ω/sq for Z1−Z6, respectively. The sheet resistance remained constant up to four coating cycles and then increased. The increase in transmittance of the composite electrode for the first four cycles is attributed to the fact that the composite electrode was repeatedly sintered to improve the crystallization of ZnO, which was justified by XRD measurements (Figure S5, Supporting Information). XRD patterns consist of separate peaks corresponding to different diffraction planes for ZnO and AgNWs. They also show the increase in intensity of peaks corresponding to ZnO with increased coating cycles. However, the transmittance of Z5 and Z6 samples was slightly decreased, which might be related to the increase in ZnO layer thickness. Moreover, evolution of sheet resistance also reflected the

sintering behavior of the composite electrode ZnO/[AgNW/ZnO]. For the first four cycles, sheet resistance was almost the same except for the change in transmittance; after that, the sheet resistance was drastically increased, which might be due to excessive sintering of AgNWs at such high temperature. Normally, the AgNWs can be heated at about 200 °C for a limited time. However, in the present work, the AgNWs were sintered at 250 °C over 20 min, which suggested that these ZnO layers might improve the stability of AgNWs. The figure of merit was calculated by using the formula[35] $\varnothing_c = T^{10}/R_s$, where T is percent transmittance at 550 nm and R_s is sheet resistance. The values of $\varnothing_c$ ($\times 10^{-3}$) were obtained as 16, 16, 18, 33, 9, and 8 for samples Z1−Z6, respectively. The maximum figure of merit of 33 $\times$ 10^{-3} was obtained for sample Z4. This indicates that only 200 nm thickness was required for the bottom ZnO layer to prepare the best ZnO/[AgNW/ZnO] electrode.

Figure 4 shows the surface morphology of ZnO/[AgNW/ZnO] composite electrode having (a) bare AgNWs and (b)

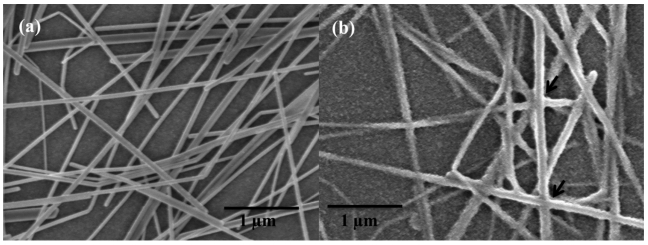

Figure 4. SEM image of the surface of ZnO/[AgNW/ZnO] composite electrode with (a) bare AgNWs on the surface without top ZnO coating and (b) covered AgNWs with top ZnO layer coating (arrows show AgNWs welding point).

AgNWs covered with ZnO. It was observed that without coating by a top ZnO layer, AgNWs remains distinct and well-separated with each other in mesh structure (Figure 4a), but after coating bya single layer of ZnO, AgNWs are connected (some points marked by arrow in Figure 4b) with each other to form a cross-linked network structure. In other words, AgNWs are welded together and the spaces between the wires are filled with ZnO. The tilted SEM micrograph of ZnO/[AgNW/ZnO] also shows the welded structure of AgNWs (some points marked by arrows in Figure S6, Supporting Information). This is the reason for enhanced conductivity of covered AgNWs with ZnO and the sheet resistance dropping from 20 to 16 Ω/sq. Recently, Kim et al.[36] have fabricated sputtered ZnO/AgNW/ZnO composite electrode with sheet resistance of 8 Ω/sq and transparency of 91.91% at 550 nm. They prepared top and bottom ZnO layers in a composite electrode by sputtering and sandwiched AgNW film between the ZnO layers. Our solution-processed electrode showed higher transparency and comparable conductivity in comparison to their vacuum-sputtered ZnO/AgNW/ZnO electrode.

A solar cell was fabricated by utilizing CIGS nanoparticles as absorber and ZnO/[AgNW/ZnO] as transparent conductive window electrode on Mo-coated glass substrate. Performance of the all-printed solar cell was evaluated by assembling ZnO/[AgNW/ZnO] composite electrode on top of solution-processed CIGS−CdS layer. Figure 5a shows the cross section image of completed cell. Some voids are visible at the buffer−window layer interface, due to removal of organic solvents from the ZnO layer during drying and annealing of the film. The current density and voltage (J−V) characteristics of all-printed CIGS solar cell are given in Figure 5b. The cell based on all printed layers exhibited efficiency of 1.6% with open circuit voltage (V_{oc}) of 0.48 V, short circuit current (J_{sc}) of 9.7 mA/cm^2, and fill factor (FF) of 34%. To evaluate the superiority of the all-layers-printed cell, another cell was also fabricated with sputtered deposited i-ZnO/ITO as top conductive window layer. The performance of the cell using bare AgNW film was also evaluated. Table 1 shows the sheet resistance and transmittance of bare AgNW film, sputtered i-ZnO/ITO, and solution-processed ZnO/[AgNW/ZnO] as window electrodes. The values of J_{sc}, V_{oc}, FF, and efficiency of solar cells prepared with these electrodes are also given in Table 1. Transmittance

Table 1. Characteristics of Transparent Conductive Oxide Electrode and Prepared Solar Cell

electrode	R_s (Ω/sq)	T (%)	J_{sc} (mA/cm^2)	V_{oc} (V)	FF	η (%)
AgNWs	11	90	1.0	0.474	0.26	0.1
i-ZnO/ITO[a]	35	90	9.0	0.475	0.31	1.3
ZnO/[AgNW/ZnO][b]	16	94	9.7	0.478	0.34	1.6

[a]Sputtered. [b]Solution-processed.

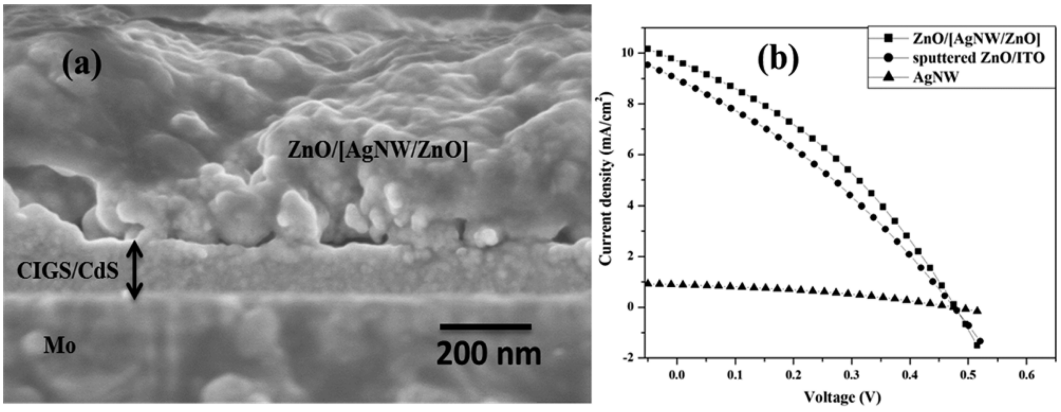

Figure 5. (a) Cross section SEM image of solar cell fabricated with solution-processed CIGS absorber, CdS buffer, and ZnO/[AgNW/ZnO] as window layers. (b) Current density and voltage (J−V) characteristics of solution-processed CIGS/CdS cells fabricated with solution-processed ZnO/[AgNW/ZnO] layer, sputtered i-ZnO/ITO film, and AgNW film as window layer.

curves for bare AgNW film and sputtered i-ZnO/ITO electrode prepared on glass are given in Figure S7 in Supporting Information. The standard solar cell with sputtered i-ZnO/ITO on CdS/CIGS/Mo/glass exhibited maximum efficiency of 1.3% with V_{oc} = 0.475 V, J_{sc} = 9.0 mA/cm^2, and FF = 31%. The device with a ZnO/[AgNW/ZnO] composite electrode exhibited comparable parameters with 1.6% efficiency, V_{oc} = 0.478 V, J_{sc} = 9.7 mA/cm^2, and FF = 34%. The device with a bare AgNW film as electrode exhibited comparable parameters with 0.1% efficiency, V_{oc} = 0.474 V, J_{sc} = 1.0 mA/cm^2, and FF = 26%. V_{oc} and J_{sc} of all-solution-processed solar cells showed higher performance than the other two cells. The solar cell prepared with only bare AgNW film as electrode exhibited very low J_{sc} of 1 mA/cm^2. Although sheet resistance of the AgNW film was 11 Ω/sq, the poor performance of the cell was attributed to the gap between the wires, which allowed very low contact area with underlying buffer layer and was also confirmed by lower FF of this cell. This provided poor charge collection by the AgNWs. When the gap between the wires was filled with ZnO layer, AgNWs were connected and welded together (Figure S5, Supporting Information) and provided larger area for charge collection. For the sputtered i-ZnO/ITO electrode, the higher sheet resistance of i-ZnO/ITO electrode might have decreased the efficiency of the cell. Thus, it is pointed out that the all layers solution-processed solar cell, with DDA-stabilized CIGS and solution-processed ZnO/[AgNW/ZnO] electrode, performed better than the sputtered deposited i-ZnO/ITO and bare AgNW film as electrodes for the same solution-processed CIGS materials.

The efficiency of our all-solution-processed DDA-stabilized CIGS solar cell is higher than the efficiency of the $CuInSe_2$ nanocrystal-based device (0.2%) first reported by Panthani et al.[15] with oleylamine-stabilized $CuInSe_2$ nanocrystals and vacuum deposited i-ZnO/ITO top contact electrode. However, the efficiency of our cell is little lower than the efficiency of device (3%) prepared by Akhavan et al.[16] with $CuInSe_2$ nanocrystals in tributylphosphine/oleylamine as solvent, which had been the highest-ever efficiency exhibited by a solar cell using as-prepared $CuInSe_2$ nanocrystal film but after vacuum annealing of completed device at 200 °C for 30 min. Despite that, the V_{oc} (0.48 V) of our device is higher than that of their device (0.41 V). The difference in microstructures of our device and theirs may also be the reason for such changes in efficiency and V_{oc}.

The series and shunt resistance of our all-solution-processed cell are 25.68 and 97.3 Ω·cm^2, respectively. The higher series resistance and lower shunt resistance is one of the reason for reduced efficiency of our cell. The higher series resistance is due to barriers at the interfaces. The voids at the interface of CIGS−CdS and ZnO/[AgNW/ZnO] (Figure 5a) may hinder some charge carriers from propagating up to the surface. The lower shunt resistance is due to the Se-deficient composition of CIGS, as dettermined by EDS (Figure 1c), which provides a shunt path for charge carriers.

In addition to the all-printed-layers solar cell, we fabricated a solar cell with DDA-stabilized CIGS and conventional i-ZnO/ITO vacuum-based window layer as discussed above. Solar cell parameters of this cell were found to be comparable with the cell based on printed ZnO/[AgNW/ZnO] window layer (Table 1), and a small decrease in efficiency was observed after replacing printed ZnO/[AgNW/ZnO] with conventional i-ZnO/ITO window layer. This analysis indicates that the CIGS layer is the main layer to decide solar cell parameters and efficiency. The difference in our CIGS layer and the CIGS layer that exhibits higher efficiency is the crystal size of CIGS. Normally, CIGS absorbers are deposited by a vacuum or high-temperature process to achieve large CIGS crystal sizes over 500 nm or even up to 1 μm.[8,17,18,37] The large grain size reduces the shunt path for photogenerated charge carriers and improves the efficiency. However, the following solution-processed buffer layer and vacuum-deposited transparent electrode deposited on the surface of the CIGS layer also affected the efficiency, due to interface adhesion between the layers. In our case, an all-solution process was used to fabricate the CIGS solar cell to increase the adhesion as much as possible. The low efficiency in our case is mainly due to the DDA-stabilized CIGS absorber, which is composed of nanoparticles of 20 nm. Although low-temperature sintering provided a smooth and partly dense film, the grain boundary serves as a potential recombination center for photogenerated charge carriers and adversely affects the solar cell performance. To improve the efficiency, optimization of the CIGS layer must be done by adjusting the sintering profile and methods to improve crystallization and densification.

4. CONCLUSIONS

We have developed a low-cost, all-layers solution-processed CIGS solar cell having 1.6% efficiency with V_{oc} = 0.48 V, J_{sc} = 9.7 mA/cm^2, and FF = 34%. For solution-processed CIGS layer deposition, CIGS nanoparticles have been synthesized in the presence of DDA as solvent and dispersant. The top conductive oxide layer with structure ZnO/[AgNW/ZnO] has been fabricated by a solution coating method with AgNW ink and ZnO precursor solutions. Our composite electrode ZnO/[AgNW/ZnO] has shown excellent conductivity with 94% transparency at 550 nm. The all-layers solution-processed cell exhibited comparable performance with sputtered i-ZnO/ITO window layer for the same DDA-stabilized CIGS materials. The demonstrated solution approach to fabricate all-layers solution-processed solar cells opens up bright chances of a low-cost, scalable technique for the absorber as well as for transparent conductive oxide window layer deposition.

■ ASSOCIATED CONTENT

Supporting Information

Seven figures showing EDS spectra of CIGS nanoparticle films, TGA curves of as-prepared CIGS nanoparticles, cross section SEM images of CIGS film and ZnO film coated on glass, XRD pattern of ZnO[AgNW/ZnO] film, SEM image of AgNW/[ZnO/AgNW] film surface, and transmittance curves. This material is available free of charge via the Internet at http://pubs.acs.org.

■ AUTHOR INFORMATION

Corresponding Authors

*E-mail msitbhu@gmail.com or manjeet@eco.sanken.osaka-u.ac.jp.

*E-mail jiu@eco.sanken.osaka-u.ac.jp.

Notes

The authors declare no competing financial interest.

■ ACKNOWLEDGMENTS

We gratefully acknowledge the help and financial support received from Solar Research Institute Inc. and COI stream project.

REFERENCES

(1) Aguilera, I.; Vida, l J.; Wahnón, P.; Reining, L.; Botti, S. First-Principles Study of the Band Structure and Optical Absorption of $CuGaS_2$. *Phys. Rev. B* **2011**, *84*, No. 085145.

(2) Jackson, P.; Hariskos, D.; Lotter, E.; Paetel, S.; Wuerz, R.; Menner, R.; Wischmann, W.; Powalla, M. New World Record for $Cu(In,Ga)Se_2$ Thin-Film Solar Cells beyond 20%. *Prog. Photovoltaics* **2011**, *19*, 894−897.

(3) Mitzi, D. B.; Yuan, M.; Liu, W.; Kellock, A. J.; Chey, S. J.; Deline, V.; Schrott, A. G. A High-Efficiency Solution-Deposited Thin-Film Photovoltaic Device. *Adv. Mater.* **2008**, *20*, 3657−3662.

(4) Mitzi, D. B. Solution Processing of Chalcogenide Semiconductors via Dimensional Reduction. *Adv. Mater.* **2009**, *21*, 3141−3158.

(5) Guo, Q.; Hillhouse, H. W.; Agrawal, R. Synthesis of Cu_2ZnSnS_4 Nanocrystal Ink and Its Use for Solar Cells. *J. Am. Chem. Soc.* **2009**, *131*, 11672−11673.

(6) Moritake, N.; Fukui, Y.; Oonuki, M.; Tanaka, K.; Uchiki, H. Preparation of Cu_2ZnSnS_4 Thin Film Solar Cells under Non-Vacuum Condition. *Phys. Status Solidi C* **2009**, *6*, 1233−1236.

(7) Todorov, T.; Mitzi, D. B. Direct Liquid Coating of Chalcopyrite Light-Absorbing Layers for Photovoltaic Devices. *Eur. J. Inorg. Chem.* **2010**, 17−28.

(8) Todorov, T.; Gunawan, O.; Gokmen, T.; Mitzi, D. B. Solution-Processed $Cu(In,Ga)(S,Se)_2$ Absorber Yielding a 15.2% Efficient Solar Cell. *Prog. Photovoltaics* **2013**, *21*, 82−87.

(9) Wang, J.-J.; Wang, Y.-Q.; Cao, F.-F.; Guo, Y.-G.; Wan, L.-J. Synthesis of Monodispersed Wurtzite Structure $CuInSe_2$ Nanocrystals and Their Application in High-Performance Organic-Inorganic Hybrid Photodetectors. *J. Am. Chem. Soc.* **2010**, *132*, 12218−12221.

(10) Tang, J.; Hinds, S.; Kelley, S. O.; Sargent, E. H. Synthesis of Colloidal $CuGaSe_2$, $CuInSe_2$, and $Cu(InGa)Se_2$ Nanoparticles. *Chem. Mater.* **2008**, *20*, 6906−6910.

(11) Ahmadi, M.; Pramana, S. S.; Lifei, X.; Chris, B.; Lam, Y. M.; Mhaisalkar, S. Evolution Pathway of CIGSe Nanocrystals for Solar Cell Applications. *J. Phys. Chem. C* **2012**, *116*, 8202−8209.

(12) Chiang, M.-Y.; Chang, S.-H.; Chen, C.-Y.; Yuan, F.-W.; Tuan, H.-Y. Quaternary $CuIn(S_{1-x}Se_x)_2$ Nanocrystals: Facile Heating-Up Synthesis, Band Gap Tuning, and Gram-Scale Production. *J. Phys. Chem. C* **2011**, *115*, 1592−1599.

(13) Suehiro, S.; Horita, K.; Kumamoto, K.; Yuasa, M.; Tanaka, T.; Fujita, K.; Shimanoe, K.; Kida, T. Solution-Processed Cu_2ZnSnS_4 Nanocrystal Solar Cells: Efficient Stripping of Surface Insulating Layers Using Alkylating Agents. *J. Phys. Chem. C* **2014**, *118*, 804−810.

(14) Dilena, E.; Xie, Y.; Brescia, R.; Prato, M.; Maserati, L.; Krahne, R.; Paolella, A.; Bertoni, G.; Povia, M.; Moreels, I.; Manna, L. $CuIn_xGa_{1-x}S_2$ Nanocrystals with Tunable Composition and Band Gap Synthesized via a Phosphine-Free and Scalable Procedure. *Chem. Mater.* **2013**, *25*, 3180−3187.

(15) Panthani, M. G.; Akhavan, V.; Goodfellow, B.; Schmidtke, J. P.; Dunn, L.; Dodabalapur, A.; Barbara, P. F.; Korgel, B. A. Synthesis of $CuInS_2$, $CuInSe_2$, and $Cu(In_xGa_{1-x})Se_2$ (CIGS) Nanocrystal "Inks" for Printable Photovoltaics. *J. Am. Chem. Soc.* **2008**, *130*, 16770−16777.

(16) Akhavan, V. A.; Panthani, M. G.; Goodfellow, B. W.; Reid, D. K.; Korgel, B. A. Thickness-Limited Performance of $CuInSe_2$ Nanocrystal Photovoltaic Devices. *Opt. Express* **2010**, *18*, A411−A420.

(17) Lauth, J.; Marbach, J.; Meyer, A.; Dogan, S.; Klinke, C.; Kornowski, A.; Weller, H. Virtually Bare Nanocrystal Surfaces: Significantly Enhanced Electrical Transport in $CuInSe_2$ and $CuIn_{1-x}Ga_xSe_2$ Thin Films upon Ligand Exchange with Thermally Degradable 1-Ethyl-5-thiotetrazole. *Adv. Funct. Mater.* **2014**, *24*, 1081−1088.

(18) Guo, Q.; Kim, S. J.; Kar, M.; Shafarman, W. N.; Birkmire, R. W.; Stach, E. A.; Agrawal, R.; Hillhouse, H. W. Development of $CuInSe_2$ Nanocrystal and Nanoring Inks for Low-Cost Solar Cells. *Nano Lett.* **2008**, *8*, 2982−2987.

(19) McCandless, B. E.; Shafarman, W. N. Chemical Surface Deposition of Ultra-thin Semiconductors. U.S. Patent US 6,537,845, March 25, 2003.

(20) Azimi, H.; Heumüller, T.; Gerl, A.; Matt, G.; Kubis, P.; Distaso, M.; Ahmad, R.; Akdas, T.; Richter, M.; Peukert, W.; Brabec, C. J. Relation of Nanostructure and Recombination Dynamics in a Low-Temperature Solution-Processed $CuInS_2$ Nanocrystalline Solar Cell. *Adv. Energy Mater.* **2013**, *3*, 1589−1596.

(21) Kim, Y. H.; Sachse, C.; Machala, M. L.; May, C.; Müller-Meskamp, L.; Leo, K. Highly Conductive PEDOT:PSS Electrode with Optimized Solvent and Thermal Post-Treatment for ITO-Free Organic Solar Cells. *Adv. Funct. Mater.* **2011**, *21*, 1076−1081.

(22) Na, S. I.; Kim, S. S.; Jo, J.; Kim, D. Y. Efficient and Flexible ITO-Free Organic Solar Cells Using Highly Conductive Polymer Anodes. *Adv. Mater.* **2008**, *20*, 4061−4067.

(23) Wu, Z.; Chen, Z.; Du, X.; Logan, J. M.; Sippel, J.; Nikolou, M.; Kamaras, K.; Reynolds, J. R.; Tanner, D. B.; Hebard, A. F.; Rinzler, A. G. Transparent, Conductive Carbon Nanotube Films. *Science* **2004**, *305*, 1273−1276.

(24) Contreras, M. A.; Barnes, T.; Lagemaat, J. V. D.; Rumbles, G.; Coutts, T. J.; Weeks, C.; Glatkowski, P.; Levitsky, I.; Peltola, J.; Britz, D. A. Replacement of Transparent Conductive Oxides by Single-Wall Carbon Nanotubes in $Cu(In,Ga)Se_2$-Based Solar Cells. *J. Phys. Chem. C* **2007**, *111*, 14045−14048.

(25) Wang, X.; Zhi, L.; Mullen, K. Transparent, Conductive Graphene Electrodes for Dye-Sensitized Solar Cells. *Nano Lett.* **2008**, *8*, 323−327.

(26) Hu, L.; Kim, H. S.; Lee, J.-Y.; Peumans, P.; Cui, Y. Scalable Coating and Properties of Transparent, Flexible, Silver Nanowire Electrodes. *ACS Nano* **2010**, *4*, 2955−2963.

(27) Zeng, X.-Y.; Zhang, Q. K.; Yu, R.-M.; Lu, C.-Z. A New Transparent Conductor: Silver Nanowire Film Buried at the Surface of a Transparent Polymer. *Adv. Mater.* **2010**, *22*, 4484−4488.

(28) Yu, Z.; Zhang, Q.; Li, L.; Chen, Q.; Niu, X.; Liu, J.; Pei, Q. Highly Flexible Silver Nanowire Electrodes for Shape-Memory Polymer Light-Emitting Diodes. *Adv. Mater.* **2011**, *23*, 664−668.

(29) Leem, D.-S.; Edwards, A.; Faist, M.; Nelson, J.; Bradley, D. D. C.; Mello, J. C. Efficient Organic Solar Cells with Solution-Processed Silver Nanowire Electrodes. *Adv. Mater.* **2011**, *23*, 4371−4375.

(30) Kim, A.; Won, Y.; Woo, K.; Jeong, S.; Moon, J. All-Solution-Processed Indium-Free Transparent Composite Electrodes Based on Ag Nanowire and Metal Oxide for Thin-Film Solar Cells. *Adv. Funct. Mater.* **2014**, *24*, 2462−2471.

(31) Chung, C. H.; Song, T. B.; Bob, B.; Zhu, R.; Duan, H.-S.; Yang, Y. Silver Nanowire Composite Window Layers for Fully Solution-Deposited Thin-Film Photovoltaic Devices. *Adv. Mater.* **2012**, *24*, 5499−5504.

(32) Singh, M.; Jiu, J.; Sugahara, T.; Suganuma, K. Photonic Sintering of Thin Film Prepared by Dodecylamine Capped $CuIn_xGa_{1-x}Se_2$ Nanoparticles for Printed Photovoltaics. *Thin Solid Films* **2014**, *565*, 11−18.

(33) Araki, T.; Jiu, J.; Nogi, M.; Koga, H.; Nagao, S.; Sugahara, T.; Suganuma, K. Low Haze Transparent Electrodes and Highly Conducting Air Dried Films with Ultra-Long Silver Nanowires Synthesized by One-Step Polyol Method. *Nano Res.* **2014**, *7*, 236−245.

(34) Jiu, J.; Nogi, M.; Sugahara, T.; Tokuno, T.; Araki, T.; Komoda, N.; Suganuma, K.; Uchida, H.; Shinozaki, K. Strongly Adhesive and Flexible Transparent Silver Nanowire Conductive Films Fabricated with a High-Intensity Pulsed Light Technique. *J. Mater. Chem.* **2012**, *22*, 23561−23567.

(35) Haacke, G. New Figure of Merit for Transparent Conductors. *J. Appl. Phys.* **1976**, *47*, 4086−4089.

(36) Kim, A.; Won, Y.; Woo, K.; Kim, C.; Moon, J. Highly Transparent Low Resistance ZnO/Ag Nanowire/ZnO Composite Electrode for Thin Film Solar Cells. *ACS Nano* **2013**, *7*, 1081−1091.

(37) Guo, Q.; Ford, G. M.; Agrawal, R.; Hillhouse, H. W. Ink Formulation and Low-Temperature Incorporation of Sodium to Yield 12% Efficient $Cu(In,Ga)(S,Se)_2$ Solar Cells from Sulfide Nanocrystal Inks. *Prog. Photovoltaics* **2013**, *21*, 64−71.